

Article

Quantitative Evaluation of Dust and Black Carbon Column Concentration in the MERRA-2 Reanalysis Dataset Using Satellite-Based Component Retrievals

Lei Li ¹, Huizheng Che ^{1,*}, Xin Su ², Xindan Zhang ¹, Ke Gui ¹, Yu Zheng ¹, Hujia Zhao ³, Hengheng Zhao ¹, Yuanxin Liang ¹, Yadong Lei ¹, Lei Zhang ¹, Junting Zhong ¹, Zhili Wang ¹ and Xiaoye Zhang ¹

¹ State Key Laboratory of Severe Weather & Key Laboratory of Atmospheric Chemistry of CMA, Chinese Academy of Meteorological Sciences, Beijing 100081, China

² Key Laboratory of Regional Ecology and Environmental Change, School of Geography and Information Engineering, China University of Geosciences, Wuhan 430074, China

³ Institute of Atmospheric Environment, Shenyang 110166, China

* Correspondence: chehz@cma.gov.cn

Abstract: The aerosol optical property products of Modern-Era Retrospective Analysis for Research and Applications, version 2 (MERRA-2) reanalysis dataset have been extensively investigated on a global or regional scale. However, the understanding of MERRA-2 aerosol component products on an extensive temporal and spatial scale is inadequate. Recently, the aerosol component products have been derived from the observations of Polarization and Directionality of the Earth’s Reflectances/Polarization and Anisotropy of Reflectance for Atmospheric Science coupled with observations from a Lidar (POLDER/PARASOL). This study presents a quantitative evaluation of the MERRA-2 reanalysis dust and black carbon (BC) column concentration using independent satellite-based aerosol component concentration retrievals. Both GRASP/Component and MERRA-2 reanalysis products can capture well the temporal variation in dust column concentration over the dust emission resource and downwind dust-dominated regions with the correlation coefficient (R) varying from 0.80 to 0.98. MERRA-2 reanalysis dust products present higher column concentration than GRASP/Component dust retrievals with relative differences of about 20~70%, except in the Taklamakan Desert and Bay of Bengal, where the relative differences can be negative. The differences in dust column concentration over the African dust regions are larger than that over the Asian dust regions. Similar temporal variations in BC column concentration are characterized by both GRASP/Component BC retrievals and MERRA-2 BC products with R of about 0.70~0.90, except in the North China Plain region. We should pay more caution with the regional applicability of MERRA-2 component products when large differences and high correlation coefficients are obtained simultaneously. The results are favorable for identifying the behavior of MERRA-2 reanalysis component estimation in a new view and demonstrate a practical application of the satellite-based component retrievals, which could make more contributions to the improvement of model estimation in the near future.



Citation: Li, L.; Che, H.; Su, X.; Zhang, X.; Gui, K.; Zheng, Y.; Zhao, H.; Zhao, H.; Liang, Y.; Lei, Y.; et al. Quantitative Evaluation of Dust and Black Carbon Column Concentration in the MERRA-2 Reanalysis Dataset Using Satellite-Based Component Retrievals. *Remote Sens.* **2023**, *15*, 388. <https://doi.org/10.3390/rs15020388>

Academic Editor: Pavel Kishcha

Received: 21 November 2022

Revised: 3 January 2023

Accepted: 4 January 2023

Published: 8 January 2023



Copyright: © 2023 by the authors. Licensee MDPI, Basel, Switzerland. This article is an open access article distributed under the terms and conditions of the Creative Commons Attribution (CC BY) license (<https://creativecommons.org/licenses/by/4.0/>).

1. Introduction

The characterizations of total aerosol optical depth (AOD) variations are extensively discussed by many researchers on a global [1–3] or regional scale [4–6] based on satellite remote sensing products derived from different instruments. The spatial and temporal distributions of aerosol optical properties associated with dust particles also have been investigated using satellite measurements in many studies. Specifically, the Total Ozone Mapping Spectrometer (TOMS) and Moderate Resolution Imaging Spectroradiometer (MODIS) are used to characterize the properties of dust aerosols and distinguish the dust

emission sources [7–9]. In addition, there are several studies focusing on the variability of dust optical depth (DOD) over the key global dust regions based on the satellite measurements, such as MODIS DOD products [10,11], Multiangle Imaging SpectroRadiometer (MISR) DODs products [12], and CALIOP DOD products [13].

Global climate models can benefit from the enhanced space-based and ground-based remote sensing observations of aerosols for further knowledge of aerosols' impacts on air quality and climate change. The assimilation of observations employed by models is helpful for an enhanced representation of aerosols [14–16]. Modern-Era Retrospective Analysis for Research and Applications, version 2 (MERRA-2) is the first multidecadal reanalysis generated from a global assimilation system developed for simultaneously assimilating meteorological and aerosol observations. MERRA-2 considers the assimilation of bias-corrected AOD from satellite observations, including MODIS, Advanced Very-High-Resolution Radiometer (AVHRR) [17], MISR [18], and Level-2 AOD of the ground-based Aerosol Robotic Network (AERONET) [19]. The significant impacts of AOD assimilation in the MERRA-2 have been demonstrated in many studies [20]. Specifically, the performance and stability of the MERRA-2 assimilation system, together with the validation of MERRA-2 AOD, have been evaluated by Randles et al., (2017) [21]. The aerosol products such as AOD, aerosol index (AI) and absorption AOD (AAOD), and PM_{2.5} have been assessed by Buchard et al., (2015, 2016, 2017) [20,22,23] using available measurements, as well as its capabilities and limitations for specific aerosol events including pollution, biomass burning, volcanic, and mineral dust events [20]. The MERRA-2 aerosol output has been extensively applied to various studies. Specifically, it can be used to forecast air quality by models [22,24], examine the interactions between aerosols and climate/weather conditions [25,26], and improve atmospheric retrievals from satellite observations [27]. A case of dust event and its transport were also investigated using the MERRA-2 data [20].

Because of inadequate constraints on emissions and insufficient knowledge of physical parameterizations (e.g., mixing, conversion, and interactions), aerosol models remain not negligibly uncertain [28,29]. The discrepancies between model estimation and observations are partly attributed to emissions inventory assumption [30,31]. For instance, several anthropogenic aerosol emissions in the key regions of China have shown decreasing trends since 2006, such as anthropogenic black carbon (BC) emission has a statistically noteworthy trend of −1.4% per year in the Peking University (PKU) inventory. However, anthropogenic BC emission in Community Emissions Data System (CEDS) inventory shows an increasing trend of 2.7% over eastern China for the period 2006–2014, which is a complete reversal of the trend of PKU inventory. Therefore, the models that employ CEDS inventory cannot successfully capture the practical descending tendency [30]. Assimilated AOD observations in MERRA-2 cannot provide sufficient information and constraints on the fractions or content of aerosol species.

Although several studies [20–23] demonstrated that the aerosol assimilation system in MERRA-2 reanalysis data could provide comparable simulations of measured aerosol properties, aerosol component products need to be assessed and validated globally by observations for further improvement due to their no constraints in the data assimilation system. AOD is observation-constrained directly by available data in MERRA-2; the evaluations of other aerosol diagnostics are more critical than AOD. Therefore, the concentration of aerosol components, which are not directly constrained by measurements during the assimilation process of MERRA-2, needs to be evaluated and validated globally in a scientific and systematic way.

This study aims to investigate the temporal differences of mineral dust and black carbon column concentration between the MERRA-2 reanalysis dataset and satellite-measured component retrievals over some regions of interest from 2005 to 2013. The innovations of this study are emphasized below regarding the contributions to the scientific community. First, this study relies on satellite-measured component retrievals and aims to validate the mineral dust and black carbon column concentration products in the MERRA-2 reanalysis dataset in detail over specific regions. The assessment is critical for understanding

MERRA-2 reanalysis of mineral dust and black carbon column concentration. Second, quite a few studies focus on validating component column concentration in the MERRA-2 reanalysis dataset rather than aerosol optical property products. Even though the pattern and amount of aerosol optical parameters are quite reasonable on a global scale, the aerosol composition products remain unvalidated due to the lack of measurements on a large scale. It should be noted that this is the first study assessing the mineral dust and black carbon column concentration across the major regions of interest over the globe, highlighting the potential role of satellite-measured retrievals and the MERRA-2 reanalysis dataset in the aerosol component studies.

The structure of this study is presented as follows. Section 2 is divided into three subsections as the description of MERRA-2 reanalysis product (Section 2.1), satellite-measured component retrievals (Section 2.2), and the regions of interest for these two components (Section 2.3). Section 3 describes results and discussions for mineral dust (Section 3.1) and BC (Section 3.2) column concentration. Finally, the main findings of the current study are summarized in Section 4. This study demonstrates a practical application of the satellite-measured component retrievals and provides the first assessment of monthly means for mineral dust and BC column concentration in the MERRA-2 over the key regions globally using satellite remote sensing observations.

2. Data and Regions

2.1. MERRA-2 Reanalysis Product

The MERRA-2, released and distributed by NASA in 2017, shows significant improvements respecting MERRA-1 [32], such as the online interaction between aerosol and radiation fields [21]. The GEOS-5 Earth system model [33] and the 3-D variational data assimilation analysis system [34] are employed in MERRA-2. A detailed description of the modeling system in MERRA-2 can be found in Gelaro et al. (2017) [35], and detailed information about the treatment of aerosols can be found in Randles et al. (2017) [21]. Major aerosol types (i.e., black carbon, organic carbon, mineral dust, inorganic salts) are estimated by the GEOS-5 model, which is coupled to the Goddard Chemistry Aerosol Radiation and Transport model (GOCART) [36,37] aerosol module. MERRA-2 reanalysis dataset, including mineral dust and black carbon column concentration products (MERRA-2 tavgM_2d_aer_Nx), can be downloaded from the Goddard Earth Sciences Data and Information Services Center (GES DISC) at <http://disc.sci.gsfc.nasa.gov/mdi/> (accessed on 1 October 2022).

2.2. Satellite-Measured Component Retrievals

Polarization and Directionality of the Earth's Reflectances/Polarization and Anisotropy of Reflectance for Atmospheric Science coupled with observations from a Lidar (POLDER/PARASOL) were launched on December 18, 2004, to obtain the information of multispectral, multidirectional, and polarized radiances and it can provide total radiance measurements at 9 wavelengths (440, 490, 565, 670, 763, 765, 865, 910, and 1020 nm) together with polarization measurements at 3 wavelengths (490, 670, and 865 nm) [38]. Recently the advanced aerosol composition products retrieved from POLDER/PARASOL by the component approach in the Generalized Retrieval of Atmosphere and Surface Properties (GRASP/Component) algorithm have been released publicly as daily, monthly, seasonal, yearly, and climatological datasets in Level-2 and Level-3 [39]. A detailed introduction to the GRASP algorithm and the specific component retrievals can be found in Dubovik et al. (2011, 2014) [40,41] and Li et al. [40], which is open-source code at <https://www.grasp-open.com>. Briefly, in the GRASP/Component approach, the refractive index of each component, together with fractions, is used by the forward model for estimating the refractive index of an aerosol mixture to simulate remote sensing measurements. Therefore, aerosol species, including black carbon, brown carbon, mineral dust, soluble inorganic salts, etc., can be obtained by the component approach [39,40]. In the current component products [39], a mixing rule of Maxwell–Garnett (MG) approximation that considers different insoluble species mixing

in the soluble host was employed for the calculation of aerosol mixture components. The quality-filtered products with the measured resolution are represented in Level-2. The products with different resolutions of 0.1° and 1° are represented in Level-3. Here, in this study, the GRASP/Component mineral dust and black carbon retrievals are re-gridded into the resolution of $0.5^\circ \times 0.625^\circ$ to compare with the corresponding MERRA-2 products using the quality-filtered GRASP/Component products with the resolution of 0.1° [39]. It is noted that based on the sensitivity tests and uncertainty assessments [39–41], the uncertainties in BC retrievals are about 50% or smaller for moderate and high aerosol loading (AOD at $440\text{ nm} \geq 0.4$) and when the proportion of BC is higher than 0.01. The estimated uncertainty for the mineral dust retrieval decreases significantly (from 100% to below 50%) when the proportion of dust is higher than 0.1. The component retrieval uncertainties are mainly associated with the refractive index of each component employed by the assumption in the component algorithm [40].

2.3. Regions of Interest

2.3.1. Dust Desert and Downwind Dust-Dominated Regions

Figure 1 shows the regions of interest for the comparisons of monthly dust column concentration between satellite-measured retrievals and MERRA-2 reanalysis data in the following assessment analysis. The monthly comparisons are performed for mineral dust column concentration over these specific regions of interest. The full names of each region, as well as the corresponding defined areas, are listed in Table 1 [42]. The regions of the Sahara Desert (SAH), Bodélé Depression (BOD), Middle East (MIE), Taklamakan Desert (TAK), and Gobi Desert (GOB) with solid rectangles represent dust emission resource regions. The regions of Eastern Tropical Atlantic (ETA), Sub-Sahel (SUS), Mediterranean Basin (MED), Arabian Sea (ARA), and Bay of Bengal (BOB) with dashed rectangles represent the important downwind dust-dominated regions.

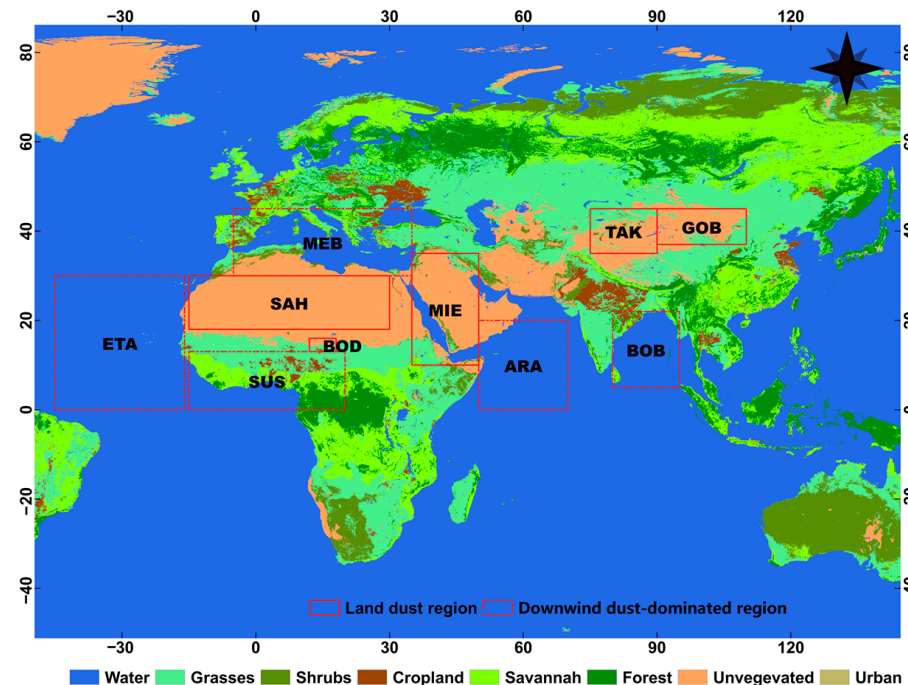


Figure 1. Regions of interest for the comparisons of monthly dust column concentration: Sahara Desert (SAH), Bodélé Depression (BOD), Middle East (MIE), Taklamakan Desert (TAK), Gobi Desert (GOB), Eastern Tropical Atlantic (ETA), Sub-Sahel (SUS), Mediterranean Basin (MED), Arabian Sea (ARA), Bay of Bengal (BOB). Solid rectangles indicate the dust emission resource regions and dashed rectangles indicate the important downwind dust-dominated regions.

Table 1. Comparison of the mineral dust and BC column concentration between MERRA-2 data and GRASP component retrievals over several key regions of interest globally [42,43].

Regions	Abbreviation	Latitude (°)	Longitude (°)
Desert areas			
Sahara Desert	SAH	18°N~30°N	15°W~30°E
Bodélé Depression	BOD	13°N~16°N	12°E~18°E
Middle East	MIE	10°N~35°N	35°E~50°E
Taklamakan Desert	TAK	35°N~45°N	75°E~90°E
Gobi Desert	GOB	37°N~45°N	90°E~110°E
Downwind dust areas			
Eastern Tropical Atlantic	ETA	0~30°N	16°W~45°W
Sub-Sahel	SUS	0~13°N	15°W~20°E
Mediterranean Basin	MED	30°N~45°N	5°W~35°E
Arabian Sea	ARA	0~20°N	50°E~70°E
Bay of Bengal	BOB	5°N~22°N	80°E~95°E
BC regions			
Sub-Sahel	SUS	0~13°N	15°W~20°E
Southern Africa	SOA	0~25°S	15°E~35°E
Northeast India	NEI	20°N~28°N	80°E~88°E
Indo-China Peninsula	ICP	15°N~25°N	90°E~110°E
North China Plain	NCP	30°N~40°N	112°E~120°E
Northeast China and East Russia	NCR	42°N~60°N	120°E~140°E

2.3.2. Biomass Burning BC

Figure 2 shows the regions of interest for the comparisons of monthly black carbon (BC) column concentration between satellite-measured retrievals and MERRA-2 reanalysis data in the following assessment analysis. The monthly comparisons are performed for BC column concentration over these specific regions of interest. The full names of each region as well as the corresponding defined areas, are also listed in Table 1 [43]. The regions of Sub-Sahel (SUS), Southern Africa (SOA), Northeast India (NEI), Indo-China Peninsula (ICP), North China Plain (NCP), and Northeast China and East Russia (NCR) with solid rectangles represent the regions of interest for the BC comparisons.

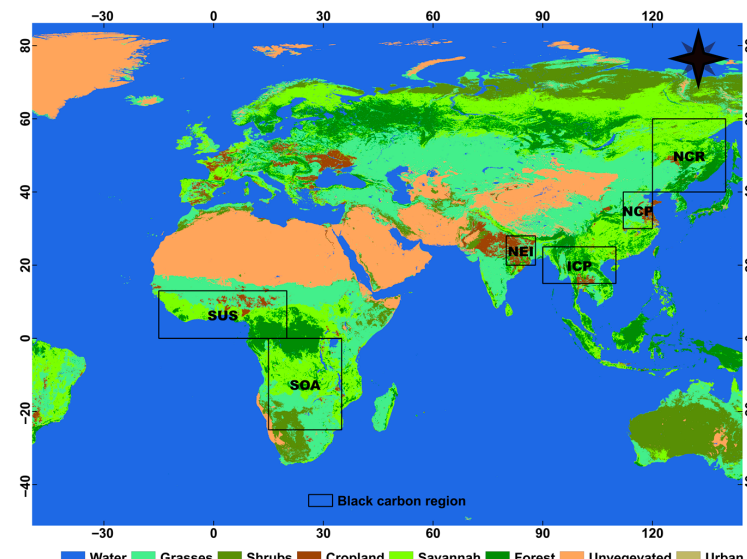


Figure 2. Regions of interest for the comparisons of monthly black carbon (BC) column concentration: Sub-Sahel (SUS), Southern Africa (SOA), Northeast India (NEI), Indo-China Peninsula (ICP), North China Plain (NCP), and Northeast China and east of Russia (NCR).

3. Results and Discussion

This section presents the comparisons of mineral dust and BC column concentration between the MERRA-2 reanalysis dataset and POLDER/GRASP component retrievals in the global key regions for the period from March 2005 to October 2013. It provides a fundamental evaluation of the quality of aerosol component reanalysis fields using the satellite-measured aerosol component concentration to examine the magnitude of mineral dust and BC column concentration because measured aerosol component concentration data were not assimilated in the MERRA-2 reanalysis.

3.1. Dust Column Concentration

There are many natural dust emission sources globally, such as the Sahara region [8,44], the Middle East, Arabian Peninsula [8,9], Taklamakan desert in northwestern China, and Gobi desert across northern China–southern Mongolia [9], etc., making dust particles have major contributions to aerosol mass loading. The prevailing winds can take the dust particles to long-distance areas up to thousands of kilometers from emission sources. For instance, the Atlantic Ocean is under the influence of dust particles emitted from the Sahara region in North Africa [45–47]. Dust aerosols also can be transported from the Sahara Desert in North Africa toward the Mediterranean and Europe [48,49]. Therefore, some key regions of dust deserts and downwind dust-dominated regions globally (shown in Figure 1) are selected to investigate the differences in mineral dust column concentration between the MERRA-2 reanalysis dataset and POLDER/GRASP component retrievals.

3.1.1. Sahara Desert

The Sahara (SAH) desert region is of great interest in the comparison of satellite-measured and MERRA-2 dust column concentrations with the most active and extensive natural dust sources. According to Figure 3, both GRASP/Component dust retrieval and MERRA-2 dust product can capture well the variation in monthly dust column concentration over the SAH region. Specifically, GRASP/Component dust retrieval and MERRA-2 dust product present the same trend of dust column concentration with high values in May, June, and July, whereas low values in November, December, and January. A good correlation coefficient ($R = 0.91$) between GRASP/Component dust retrieval and MERRA-2 dust product is obtained in the SAH region with $RMSE = 237.67 \text{ mg/m}^2$ (in Table 2). It is noted that MERRA-2 dust concentrations are higher than GRASP/Component dust concentrations for all months in Figure 3. The differences in regional means between these two products can be found in Table 3. We can see that MERRA-2 overestimates dust column concentration in the SAH region throughout the year compared to GRASP/Component dust retrieval with the maximum absolute difference in June (305.9 mg/m^2) and the maximum relative difference in November (62.8%). The absolute minimum difference is obtained in January (116.4 mg/m^2), and the minimum relative difference is obtained in August (39.2%). The differences could be associated with the estimation of some meteorological parameters (such as precipitation [50] and wind speed [4]) in the MERRA-2 reanalysis system that makes significant contributions to the magnitude of dust column concentration.

Table 2. The statistics for the comparisons of monthly dust column concentration between MERRA-2 data and POLDER/GRASP component products over the regions of interest. R indicates the correlation coefficient, and RMSE indicates root mean square error.

Desert Region	R	RMSE (mg/m^2)	Downwind Dust Region	R	RMSE (mg/m^2)
SAH	0.91	237.67	ETA	0.92	86.79
BOD	0.88	412.36	SUS	0.89	159.08
MIE	0.90	134.43	MED	0.88	82.34
TAK	0.80	122.30	ARA	0.98	89.48
GOB	0.84	74.36	BOB	0.84	29.61

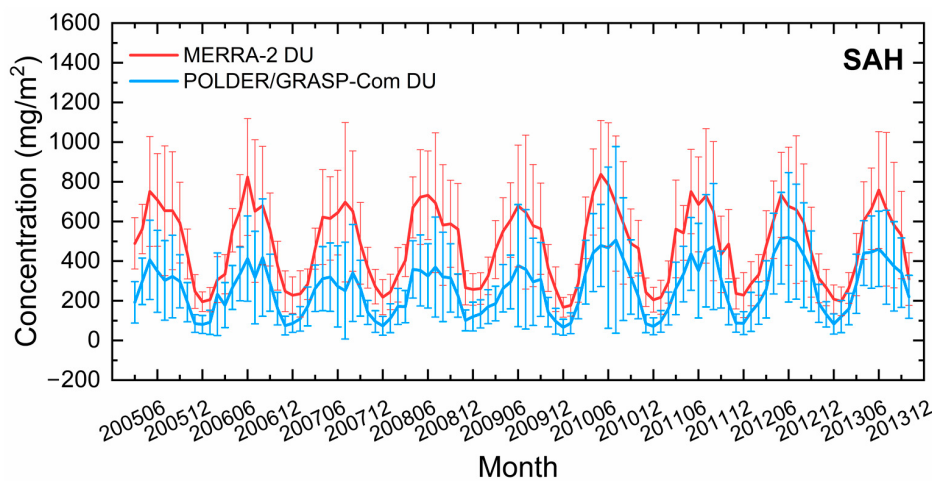


Figure 3. The monthly comparisons of dust column concentration between MERRA-2 data and POLDER/GRASP component product over Sahara Desert (SAH) region during the period from 2005 March to 2013 October. Red line represents MERRA-2 data, blue line represents POLDER/GRASP component product, and the error bars indicate the standard deviation (STD), respectively.

Table 3. The regional differences (Diff.) of dust column concentration for the monthly means during the period March 2005 to October 2013 between MERRA-2 data and POLDER/GRASP component products. Absolute differences (mg/m^2) represent MERRA-2 dust minus POLDER/GRASP dust, and relative differences (mg/m^2) represent the differences between MERRA-2 dust and POLDER/GRASP dust divided by MERRA-2 dust.

Month	SAH Diff.		BOD Diff.		MIE Diff.		TAK Diff.		GOB Diff.	
	mg/m^2	%	mg/m^2	%	mg/m^2	%	mg/m^2	%	mg/m^2	%
Jan.	116.4	51.0	352.5	52.9	73.5	39.4	-6.8	-4.8	13.1	13.8
Feb.	122.8	40.6	369.2	47.0	54.0	19.4	7.9	3.2	34.8	22.1
Mar.	222.0	48.3	399.8	40.0	100.5	27.7	-56.3	-13.4	44.1	17.9
Apr.	256.8	42.3	379.6	34.3	88.6	20.6	-60.5	-11.3	35.9	11.8
May	305.9	43.4	479.1	44.7	90.7	18.0	53.6	9.4	98.3	31.6
Jun.	328.4	45.5	424.5	42.7	170.9	28.5	124.5	23.7	113.0	43.2
Jul.	289.7	42.9	470.8	54.2	189.3	33.1	24.7	7.0	82.9	41.1
Aug.	242.6	39.2	330.3	51.9	209.7	45.8	144.7	32.4	90.7	48.5
Sep.	211.1	40.5	302.2	49.0	117.8	33.7	141.7	35.8	63.9	39.4
Oct.	222.2	54.3	463.5	61.1	115.2	44.5	126.3	49.2	74.1	52.1
Nov.	159.8	62.8	428.9	67.7	101.0	55.9	55.3	35.3	49.9	44.6
Dec.	130.1	60.9	390.7	63.1	68.8	43.0	38.8	31.3	23.5	26.4
Jan.	42.5	34.7	171.1	45.0	29.7	41.4	15.4	30.8	-9.2	-47.3
Feb.	46.6	38.6	248.8	44.6	43.5	38.3	30.9	37.9	1.6	4.7
Mar.	87.0	46.1	330.3	44.8	112.4	60.0	46.2	41.4	27.2	39.8
Apr.	70.0	45.7	143.5	28.1	131.5	55.5	59.4	42.8	25.4	27.7
May	99.4	49.9	71.8	19.5	109.4	49.5	49.4	35.1	1.4	1.0
Jun.	129.3	53.6	13.5	4.1	94.7	50.7	155.6	42.1	-37.1	-29.6
Jul.	140.0	53.1	36.1	22.4	69.8	45.7	186.8	42.8	-9.8	-8.3
Aug.	107.2	51.4	19.0	20.0	60.9	46.0	109.2	44.2	-24.6	-35.1

Table 3. Cont.

Month	SAH Diff.		BOD Diff.		MIE Diff.		TAK Diff.		GOB Diff.	
	mg/m ²	%								
Sep.	61.3	41.0	15.5	9.8	56.5	40.7	66.0	39.3	-37.7	-114.2
Oct.	41.7	36.3	97.3	39.2	65.5	55.1	25.2	36.7	-26.0	-137.6
Nov.	15.3	20.5	93.7	38.9	45.2	53.5	15.4	36.2	-17.0	-133.0
Dec.	19.5	25.0	115.6	44.0	31.6	47.0	9.2	21.8	-19.7	-177.8

3.1.2. Bodélé Depression

As one of the strongest dust emission sources [8], the Bodélé Depression (BOD) region has the most interesting for the investigation of the discrepancies among different products. Figure 4 presents the differences in dust column concentration between GRASP/Component dust retrieval and MERRA-2 dust product over the BOD area. It is evident that both GRASP/Component dust retrieval and MERRA-2 dust product can capture well the variation in monthly dust column concentration over the BOD region. Specifically, GRASP/Component dust retrieval and MERRA-2 dust product present the same trend of dust column concentration with extremely high values from March to June. A good correlation coefficient ($R = 0.88$) between GRASP/Component dust retrieval and MERRA-2 dust product is obtained in the BOD region with RMSE = 412.36 mg/m² (in Table 2). It is noted that MERRA-2 dust concentrations are higher than GRASP/Component dust concentrations for all months in Figure 4. The differences in regional means between these two products can be found in Table 3. We can see that MERRA-2 overestimates dust column concentration in the BOD region throughout the year compared to GRASP/Component dust retrieval with the maximum absolute difference in May (479.1 mg/m²) and a maximum relative difference in November (67.7%). The absolute minimum difference of 302.2 mg/m² was recorded in September, and the minimum relative difference was obtained in April (34.3%).

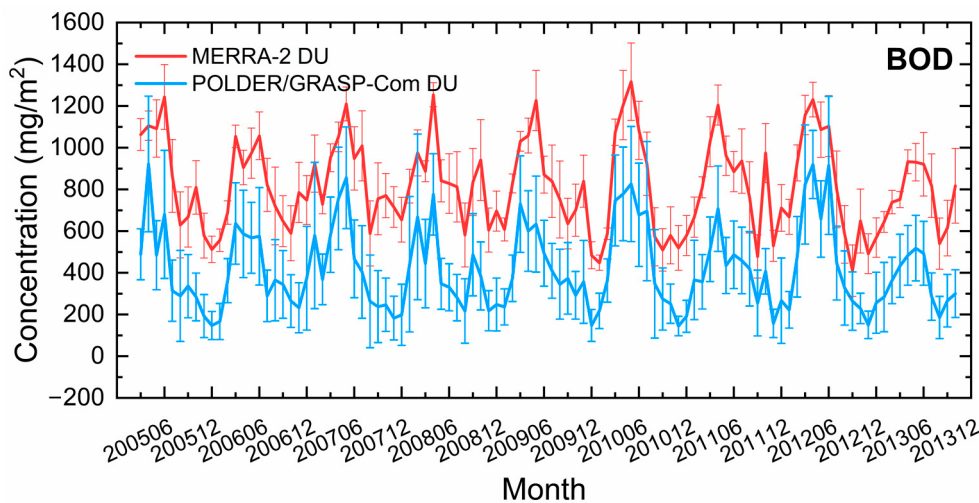


Figure 4. Same as Figure 3, but for Bodélé Depression (BOD) region.

3.1.3. Middle East

The dust concentration over the Middle East (MIE) region also presents significant interannual variation. The differences in column dust concentration between GRASP/Component dust retrieval and MERRA-2 dust product over MIE are shown in Figure 5. On a regional means, the temporal variations represented by GRASP/Component dust retrieval and MERRA-2 dust product are in very good agreement. Specifically, GRASP/Component dust retrieval and MERRA-2 dust product present the same trend of dust column con-

centration with high values in May, June, and July, whereas low values in November, December, and January. The statistics in the comparisons are also investigated for the regional dust column concentration. A good correlation coefficient ($R = 0.90$) between GRASP/Component dust retrieval and MERRA-2 dust product is obtained in the MIE region with RMSE = 134.43 mg/m^2 (in Table 2). It is worth mentioning that MERRA-2 dust concentrations are higher than GRASP/Component dust concentrations for all months in Figure 5. The differences in regional means between these two products can be found in Table 3. We can see that MERRA-2 overestimates dust column concentration in the MIE region throughout the year compared to GRASP/Component dust retrieval, with the maximum absolute difference in August (209.7 mg/m^2) and the relative difference in November (55.9%). The absolute minimum difference is obtained in February (54.0 mg/m^2) and the relative difference in May (18.0%). We should point out that the highest dust column concentration in the MIE region was retrieved in 2012 (Figure 5), which is consistent with the findings that the maximum values of AOD observed in 2012 over the MIE region using MODIS products during the period 2000 to 2015 [5]. The meteorological parameters of sea level pressure and wind speed representing the influences of synoptic systems on dust concentration make contributions to aerosol loading in the MIE region. The variation in dust column concentration in the Arabian Peninsula is intensely associated with the Shamal winds, the magnitude of precipitation, the tropical Indian Ocean, and the Mediterranean Sea temperatures [51]. The accuracy of meteorological parameters estimation in the MERRA-2 reanalysis system could partly affect the differences.

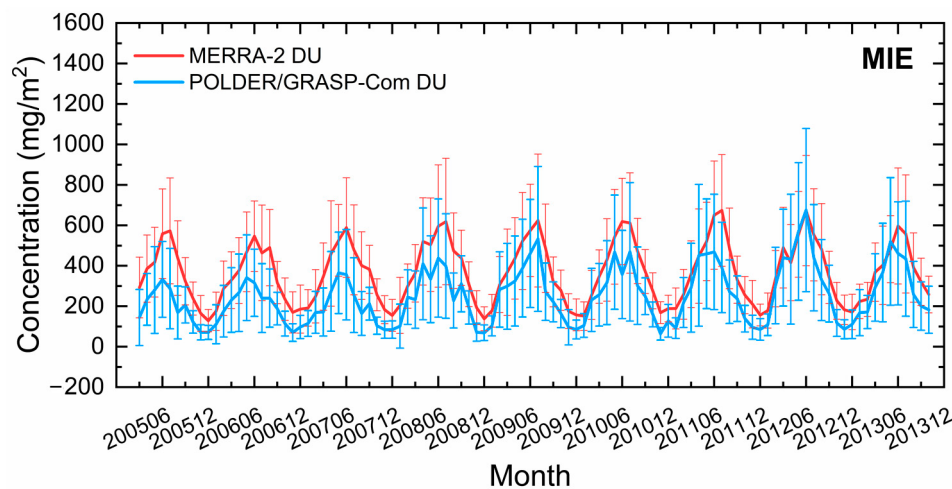


Figure 5. Same as Figure 3, but for Middle East (MIE) region.

3.1.4. Taklamakan Desert

The comparison of the Taklamakan (TAK) desert in northwestern China is shown in Figure 6. We can see that the same variation in monthly means for the calculation of regional values is reflected by both GRASP/Component dust retrieval and MERRA-2 dust product. Specifically, GRASP/Component dust retrieval and MERRA-2 dust product present the same trend of dust column concentration with high values in April and May, whereas there are low values in November, December, and January. A correlation coefficient of 0.80 is found between GRASP/Component dust retrieval and MERRA-2 dust product in the TAK region with RMSE = 122.30 mg/m^2 (in Table 2). The differences in regional means between these two products can be found in Table 3. We can see that over the TAK region, the dust column concentration of MERRA-2 is higher than those of GRASP/Component dust retrieval from May to December and February; however, it is lower for the months of January, March, and April. The maximum absolute differences of 144.7 mg/m^2 and 141.7 mg/m^2 are obtained in August and September, respectively, and the maximum relative difference is recorded in October (49.2%). The absolute minimum difference was obtained in January (-6.8 mg/m^2 indicating MERRA-2 dust column concentration is lower

than GRASP/Component dust column concentration), and a minimum relative difference of 3.2% was recorded in February.

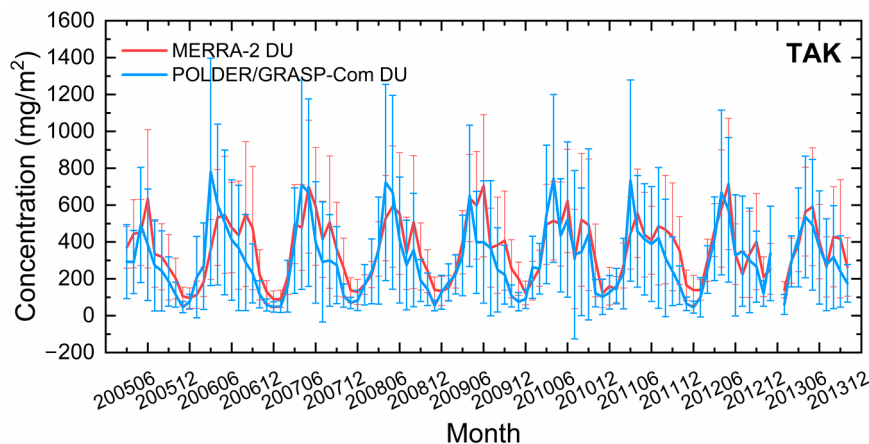


Figure 6. Same as Figure 3, but for Taklamakan Desert (TAK) region.

3.1.5. Gobi Desert

The comparison of the Gobi Desert (GOB) region covering the northern part of China and the southern sector of Mongolia is shown in Figure 7. At a regional level, both GRASP/Component dust retrieval and MERRA-2 dust product can capture well the variation in monthly dust column concentration over the GOB region. Specifically, GRASP/Component dust retrieval and MERRA-2 dust product present the same trend of dust column concentration with high values in April and May, whereas low values in December and January. The correlation coefficient of 0.84 and RMSE = 74.36 mg/m² are recorded between GRASP/Component dust retrieval and MERRA-2 dust product in the GOB region (Table 2). The differences in regional means between these two products can be found in Table 3. We can see that MERRA-2 overestimates dust column concentration in the GOB region throughout the year compared to GRASP/Component dust retrieval, with the maximum absolute difference in June (113.0 mg/m²) and a maximum relative difference in October (52.1%). The absolute minimum difference is obtained in January (13.1 mg/m²), and the minimum relative difference of 11.8% is recorded in April.

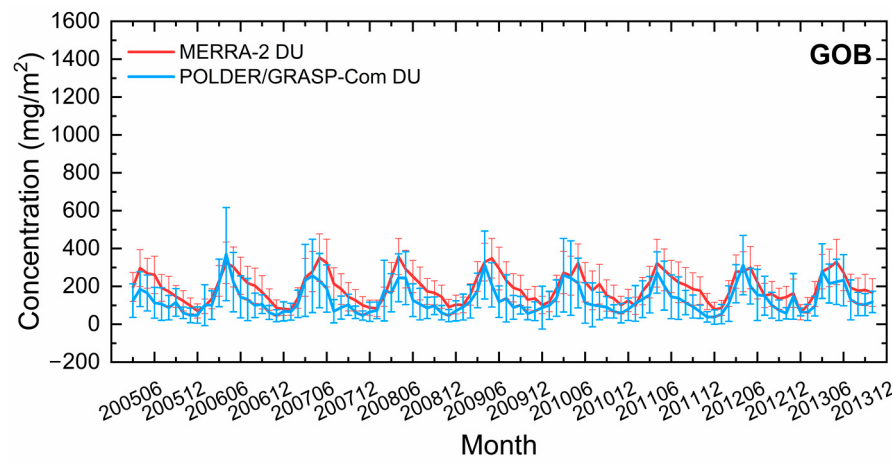


Figure 7. Same as Figure 3, but for Gobi Desert (GOB) region.

3.1.6. Eastern Tropical Atlantic

The accuracy of dust column concentration in downwind regions over the globe also needs to be examined. The intra-annual and interannual variations in dust column concentration have distinctive cycles that are determined by the source or downwind

region [52]. The dust particles over the tropical Atlantic Ocean are transported from the Sahara by tropical cyclones [53,54]. Dust particles originating from North Africa are also observed over the Caribbean Sea [42,55]. Therefore, we investigate the differences in dust column concentration over the Eastern Tropical Atlantic (ETA) region for these two products. Similar variations in monthly means for the calculation of regional values are reflected by both GRASP/Component dust retrieval and MERRA-2 dust product (Figure 8), with high values in June and July, whereas low values are in November and December. This behavior is consistent regardless of the differences observed, with a maximum absolute difference in July (140.0 mg/m²) and a maximum relative difference in June and July (about 53%); the absolute minimum difference and relative differences are obtained in November (15.3 mg/m² and 20.5%, respectively) (Table 3). A good correlation coefficient ($R = 0.92$) between GRASP/Component dust retrieval and MERRA-2 dust product is obtained in the ETA region with RMSE = 86.79 mg/m² (in Table 2). The differences could be partly attributed to the estimation of dust source emission intensity and their long-distance transport in the MERRA-2 reanalysis system.

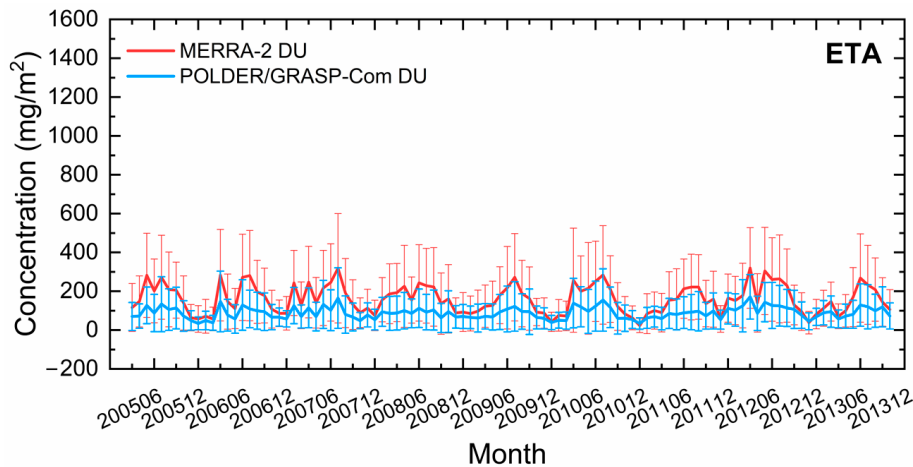


Figure 8. Same as Figure 3, but for Eastern Tropical Atlantic (ETA) region.

3.1.7. Sub-Sahel

The transatlantic transport of dust particles originating from Saharan and North Africa has been investigated by many studies [56,57]. For instance, during boreal winter, relatively high dust concentrations are observed over the Gulf of Guinea and across the northern regions (from Ghana to Cameroon) that are transported by the Harmattan from Saharan dust [52,58]. Therefore, we also selected the Sub-Sahel (SUS) region as a region of interest for the comparisons (Figure 9). As shown in Figure 9, both GRASP/Component dust retrieval and MERRA-2 dust product can capture well the variation in monthly dust column concentration over the SUS region. Specifically, GRASP/Component dust retrieval and MERRA-2 dust product present the same trend of dust column concentration with high values in February, March, and April, whereas low values in August. A good correlation coefficient ($R = 0.89$) between GRASP/Component dust retrieval and MERRA-2 dust product is obtained in the SUS region with RMSE = 159.08 mg/m² (in Table 2). It is noted that MERRA-2 dust concentrations are higher than GRASP/Component dust concentrations for all months in Figure 9. The differences in regional means between these two products can be found in Table 3. We can see that MERRA-2 overestimates dust column concentration in the SUS region throughout the year compared to GRASP/Component dust retrieval, with the maximum absolute difference in March (330.3 mg/m²) and the relative difference in January (45.0%). The absolute minimum difference and relative difference were recorded simultaneously in June (116.4 mg/m², 39.2%, respectively).

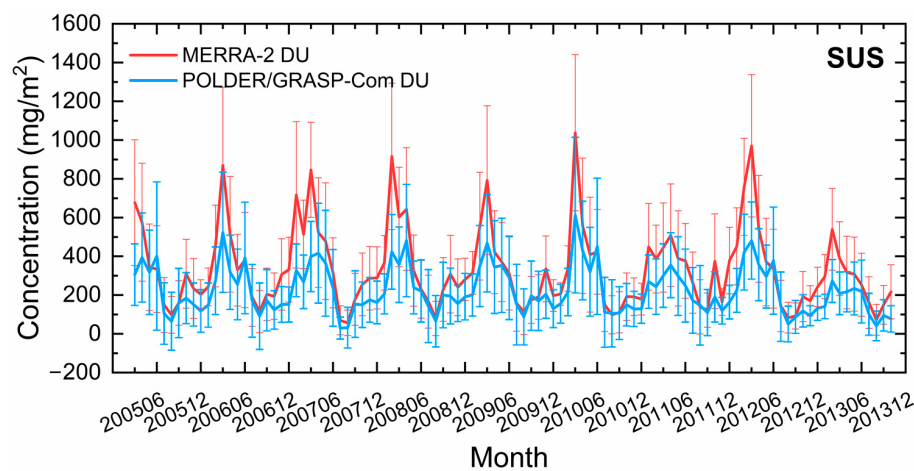


Figure 9. Same as Figure 3, but for Sub-Saharan Sahel (SUS) region.

3.1.8. Mediterranean Basin

Aerosol loadings and types over the Mediterranean Basin (MED) region present interannual variations [6]. Mineral dust particles emitted from the Saharan and Middle Eastern deserts to the Mediterranean are demonstrated by the observations [6,49,52,59], which can be attributed to the nocturnal low-level jets, Harmattan surge, and Mediterranean depressions [60,61]. Figure 10 shows the comparison of dust column concentration between GRASP/Component dust retrieval and MERRA-2 dust product in the MED region. We can see that both GRASP/Component dust retrieval and MERRA-2 dust product can capture well the variation in monthly dust column concentration over the MED region. Specifically, in the MED region, high dust column concentrations are revealed by both GRASP/Component dust retrievals and MERRA-2 dust products in April and May, as well as low values recorded in November, December, and January. A good correlation coefficient ($R = 0.88$) between GRASP/Component dust retrieval and MERRA-2 dust product is obtained in the MED region with RMSE = 82.34 mg/m² (in Table 2). It is noted that MERRA-2 dust concentrations are higher than GRASP/Component dust concentrations for all months in Figure 10. The differences in regional means between these two products can be found in Table 3. We can see that MERRA-2 overestimates dust column concentration in the MED region throughout the year compared to GRASP/Component dust retrieval, with the maximum absolute difference in April (131.5 mg/m²) and the maximum relative difference in March (60.0%). The absolute minimum difference was obtained in January (29.7 mg/m²), together with a minimum relative difference of 38.3% in February. The estimation of nocturnal low-level jets, Harmattan surge, and Mediterranean depressions in the model employed by MERRA-2 could make contributions to the differences.

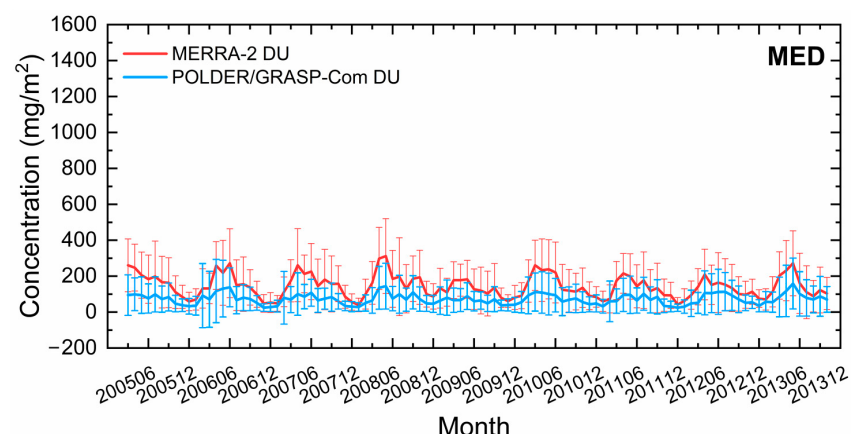


Figure 10. Same as Figure 3, but for Mediterranean Basin (MED) region.

3.1.9. Arabian Sea

The differences in dust column concentration over the Arabian Sea (ARA) region are presented in Figure 11. On a regional means, the temporal variation in dust column concentration between GRASP/Component dust retrieval and MERRA-2 dust product is in very good agreement over the ARA region. Specifically, GRASP/Component dust retrieval and MERRA-2 dust product present the same trend of dust column concentration with high values in June and July, whereas there are low values in November, December, and January. The statistics in the comparisons are also investigated for the regional dust column concentration (in Table 2). A good correlation coefficient ($R = 0.98$) between GRASP/Component dust retrieval and MERRA-2 dust product is obtained in the ARA region with $RMSE = 89.48 \text{ mg/m}^2$. It is noted that MERRA-2 dust concentrations are higher than GRASP/Component dust concentrations for all months in Figure 11. The differences in regional means between these two products can be found in Table 3. We can see that MERRA-2 overestimates dust column concentration in the ARA region throughout the year compared to GRASP/Component dust retrieval, with the maximum absolute difference in July (186.8 mg/m^2) and the relative difference in August (44.2%). The absolute minimum difference and relative difference were recorded simultaneously in December (9.2 mg/m^2 and 21.8%, respectively).

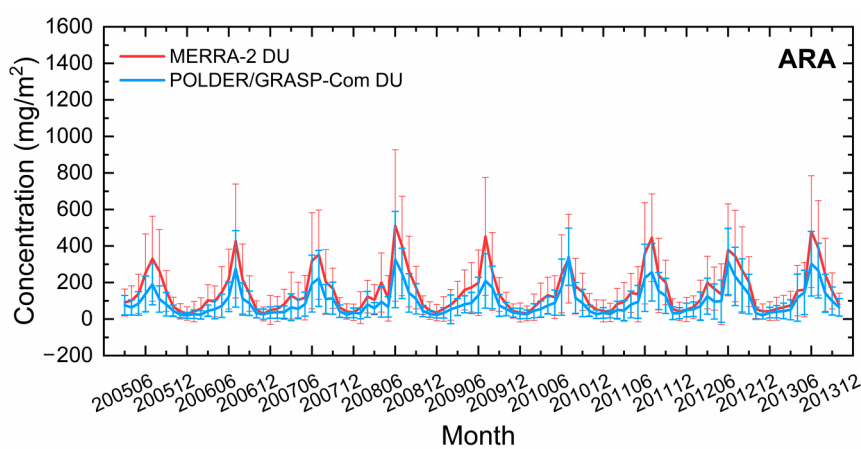


Figure 11. Same as Figure 3, but for Arabian Sea (ARA) region.

3.1.10. Bay of Bengal

Figure 12 presents the comparisons of dust column concentration over another downwind Bay of Bengal (BOB) region. As shown in Figure 12, both GRASP/Component dust retrieval and MERRA-2 dust product can capture well the variation in monthly dust column concentration over the BOB region. Specifically, GRASP/Component dust retrieval and MERRA-2 dust product present the same trend of dust column concentration with high values in May, June, and July. However, low values are retrieved in November, December, and January from satellite observations, whereas low values are obtained in October, November, and December from the MERRA-2 dataset. The correlation coefficient of $R = 0.84$ together with $RMSE = 29.61 \text{ mg/m}^2$ (in Table 2) is found between GRASP/Component dust retrieval and MERRA-2 dust product in the BOB region. The differences in regional means between these two products can be found in Table 3. We can see that over the BOB region, the dust column concentration of MERRA-2 is higher than those of GRASP/Component dust retrieval from February to May; however, lower concentration for other months (from June to January). The maximum absolute differences of -37.7 mg/m^2 and -37.1 mg/m^2 (negative values indicate MERRA-2 dust column concentration is lower than GRASP/Component dust column concentration) are obtained in September and June, respectively, as well as the maximum relative difference of -177.8% (negative values indicate MERRA-2 dust column concentration are lower than GRASP/Component dust column concentration) is obtained

in December. The absolute minimum difference and relative difference (1.4 mg/m^2 and 1.0%, respectively) were obtained in May.

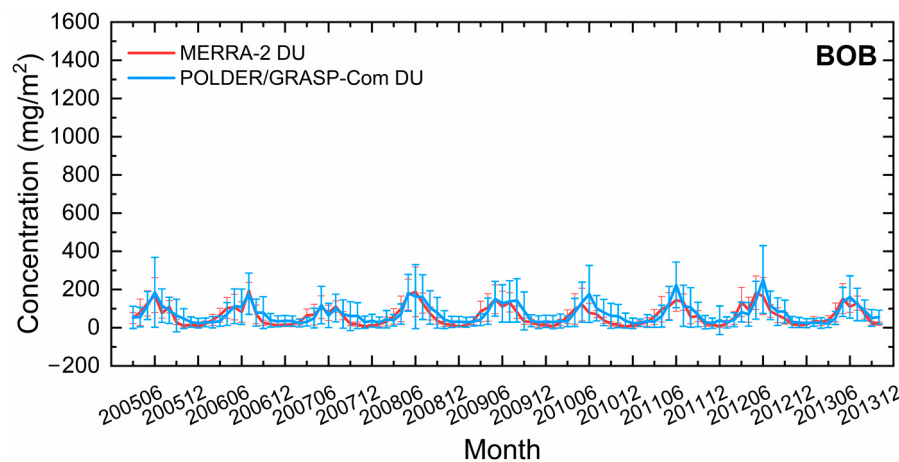


Figure 12. Same as Figure 3, but for Bay of Bengal (BOB) region.

3.2. BC

Over the biomass burning and BC-affected areas in the globe, the comparisons are conducted over several regions of interest such as Sub-Saharan (SUS), Southern Africa (SOA), Northeast India (NEI), Indo-China Peninsula (ICP), North China Plain (NCP), and Northeast China and east of Russia (NCR) shown in Figure 2 to investigate the differences of BC column concentration between the MERRA-2 reanalysis dataset and POLDER/GRASP component retrievals.

3.2.1. Sub-Saharan

Figure 13 presents the comparisons of BC column concentration over the Sub-Saharan (SUS) region. We can see that both GRASP/Component BC retrieval and MERRA-2 BC product can capture well the variation in monthly BC column concentration over the SUS region. Specifically, GRASP/Component BC retrieval and MERRA-2 BC product presents the same trend of BC column concentration with high values in December and January and low values in April and May. The statistics in the comparisons for the regional BC column concentration are listed in Table 4. A good correlation coefficient ($R = 0.92$) and low RMSE = 0.66 mg/m^2 are recorded between GRASP/Component BC retrieval and MERRA-2 BC product in the SUS region. The differences in regional means between these two products can be found in Table 5. It is worth mentioning that over the SUS region, the BC column concentration of MERRA-2 is higher than those of GRASP/Component BC retrieval from March to November; however, lower during the months of December, January, and February. The maximum absolute difference of -1.0 mg/m^2 (negative values indicate MERRA-2 BC column concentration is lower than GRASP/Component BC column concentration) is obtained in January, as well as the maximum relative difference of 70.5% is obtained in May. The absolute minimum difference and relative difference (0.1 mg/m^2 and 4.1%, respectively) were obtained in August.

Table 4. The statistics for the comparisons of monthly BC column concentration between MERRA-2 data and POLDER/GRASP component products over the regions of interest. R indicates the correlation coefficient and RMSE indicates root mean square error.

BC Region	R	RMSE (mg/m ²)	BC Region	R	RMSE (mg/m ²)
SUS	0.92	0.66	ICP	0.89	1.30
SOA	0.94	0.77	NCP	0.46	3.88
NEI	0.72	2.31	NCR	0.68	0.75

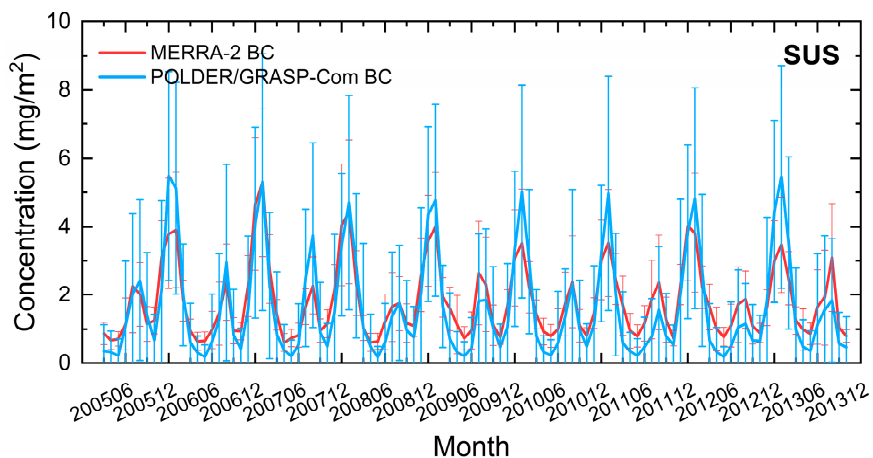


Figure 13. The monthly comparisons of BC column concentration between MERRA-2 data and POLDER/GRASP component product over Sub-Sahel (SUS) region during the period from 2005 March to 2013 October. Red line represents MERRA-2 data, blue line represents POLDER/GRASP component product, and the error bars indicate the standard deviation (STD), respectively.

Table 5. The regional differences (Diff.) of BC column concentration for the monthly means during the period March 2005 to October 2013 between MERRA-2 data and POLDER/GRASP component products. Absolute differences (mg/m^2) represent MERRA-2 BC minus POLDER/GRASP BC, and relative differences (mg/m^2) represent the differences between MERRA-2 BC and POLDER/GRASP BC divided by MERRA-2 BC.

Month	SUS Diff.		SOA Diff.		NEI Diff.		ICP Diff.		NCP Diff.		NCR Diff.	
	mg/m^2	%	mg/m^2	%	mg/m^2	%	mg/m^2	%	mg/m^2	%	mg/m^2	%
Jan.	-1.0	-25.7	0.7	39.5	3.2	60.4	1.7	65.7	4.5	74.0	0.2	25.2
Feb.	-0.2	-9.8	0.5	46.4	2.7	67.3	1.5	47.7	4.5	77.0	0.2	18.5
Mar.	0.6	44.2	0.3	49.0	2.5	75.3	1.7	30.7	4.0	79.6	0.8	59.2
Apr.	0.5	55.3	0.3	53.3	2.3	76.2	0.7	21.0	4.0	84.7	0.6	24.4
May	0.5	70.5	0.4	38.4	2.0	73.4	0.7	47.0	3.5	73.2	0.4	19.1
Jun.	0.4	39.2	0.4	19.1	1.9	78.8	0.5	48.7	1.7	31.3	0.9	54.1
Jul.	0.4	18.6	-0.2	-6.5	1.4	84.3	0.4	47.1	3.7	80.4	1.1	67.4
Aug.	0.1	4.1	0.0	0.2	1.5	81.6	0.8	61.6	3.7	86.4	0.8	66.9
Sep.	0.2	17.1	-0.2	-4.4	1.7	83.5	1.2	71.8	3.6	78.7	0.4	43.3
Oct.	0.4	39.8	1.0	32.5	2.1	66.4	1.6	77.4	4.2	74.9	0.7	56.0
Nov.	0.5	22.3	0.7	52.8	2.9	58.1	1.4	75.5	4.3	79.8	0.8	66.5
Dec.	-0.4	-10.3	0.7	55.8	3.5	58.0	1.5	68.9	3.9	73.3	-0.2	-13.6

3.2.2. Southern Africa

The comparisons of BC column concentration in the Southern Africa (SOA) region between GRASP/Component BC retrieval and MERRA-2 BC product are shown in Figure 14. Similar variations in monthly means for the regional BC column concentration are reflected by both GRASP/Component retrievals and MERRA-2 products over the SOA region. Specifically, GRASP/Component BC retrieval and MERRA-2 BC products present the highest concentration in August and September, while the lowest concentration is in March and April. A good correlation coefficient ($R = 0.94$) and low RMSE = $0.77 \text{ mg}/\text{m}^2$ are obtained between GRASP/Component BC retrieval and MERRA-2 BC product in the SOA region. The differences in regional means between these two products can be found in Table 5. We can see that over the SOA region, the BC column concentration of MERRA-2 is higher than those of GRASP/Component BC retrieval in all months except July, August, and September when the biomass burning is strong. The maximum absolute difference of $1.0 \text{ mg}/\text{m}^2$ was obtained in October, and the maximum relative difference of 55.8%

was obtained in December. The BC column concentration over the SOA region in August, reflected by GRASP/Component retrievals and MERRA-2 products, are almost the same.

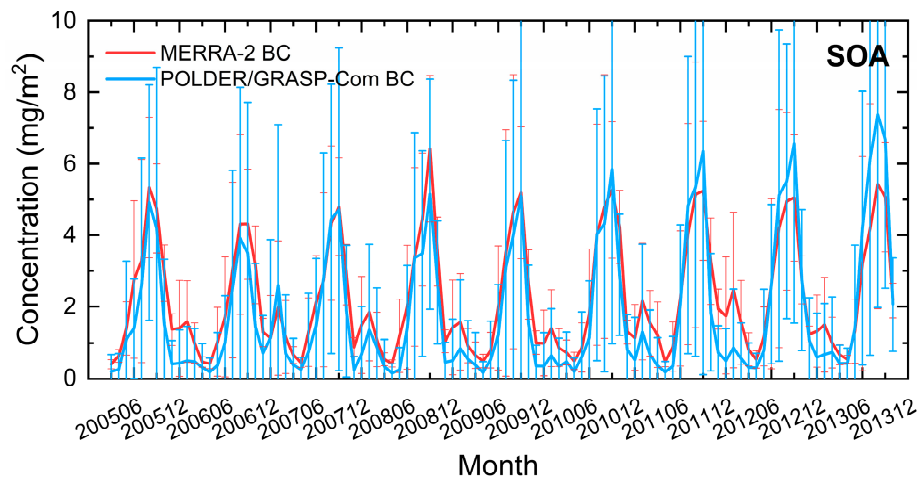


Figure 14. Same as Figure 13, but for Southern Africa (SOA) region.

3.2.3. Northeast India

Figure 15 shows the comparisons of BC column concentration in Northeast India (NEI) region between GRASP/Component BC retrieval and MERRA-2 BC product. As shown in Figure 15, both GRASP/Component BC retrieval and MERRA-2 BC product can capture well the variation in monthly BC column concentration over the NEI region. Specifically, GRASP/Component BC retrieval and MERRA-2 BC product presents the same trend of BC column concentration with high values in November, December, and January, whereas low values in July, August, and September. The correlation coefficient of $R = 0.72$ together with RMSE = 2.31 mg/m^2 (in Table 4) is found between GRASP/Component BC retrieval and MERRA-2 BC product in the NEI region. The differences in regional means between these two products can be found in Table 5. We can see that over the NEI region, the BC column concentration of MERRA-2 presents approximately 60~85% higher than those of GRASP/Component BC retrieval throughout the year. The absolute minimum difference of 1.4 mg/m^2 is recorded in July when BC column concentration reaches the lowest values reflected by both GRASP/Component BC retrieval and MERRA-2 BC product.

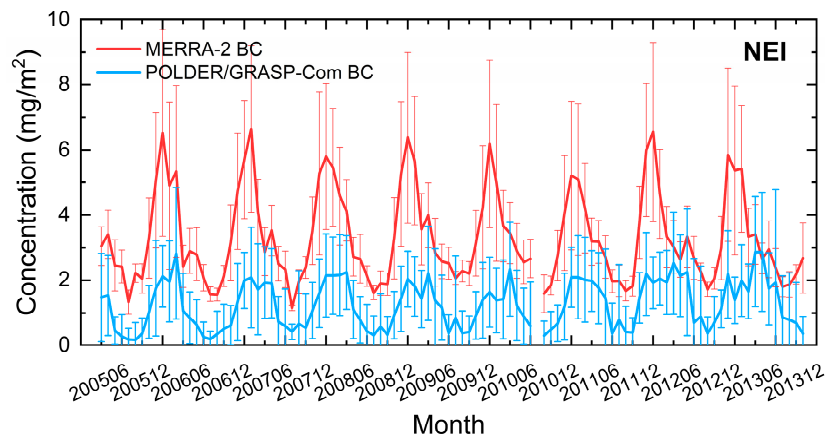


Figure 15. Same as Figure 13, but for Northeast India (NEI) region.

3.2.4. Indo-China Peninsula

The comparisons of BC column concentration between GRASP/Component BC retrieval and MERRA-2 BC over the Indo-China Peninsula (ICP) region are represented in Figure 16. The temporal variation in monthly BC column concentration over the ICP region

for the calculation of regional means is reflected by both GRASP/Component dust retrieval and MERRA-2 dust product with good consistencies. Specifically, GRASP/Component BC retrieval and MERRA-2 BC product present very high BC column concentration in April and May, whereas low BC column concentration in July. The correlation coefficient of $R = 0.89$ together with $RMSE = 1.30 \text{ mg/m}^2$ (in Table 4) are obtained between GRASP/Component BC retrieval and MERRA-2 BC product in the ICP region. The differences in regional means between these two products can be found in Table 5. We can see that over the ICP region, the BC column concentration of MERRA-2 is higher than those of GRASP/Component BC retrieval throughout the year, with the absolute differences varying from 0.4 mg/m^2 to 1.7 mg/m^2 and the relative differences varying from 21.0% to 77.4%.

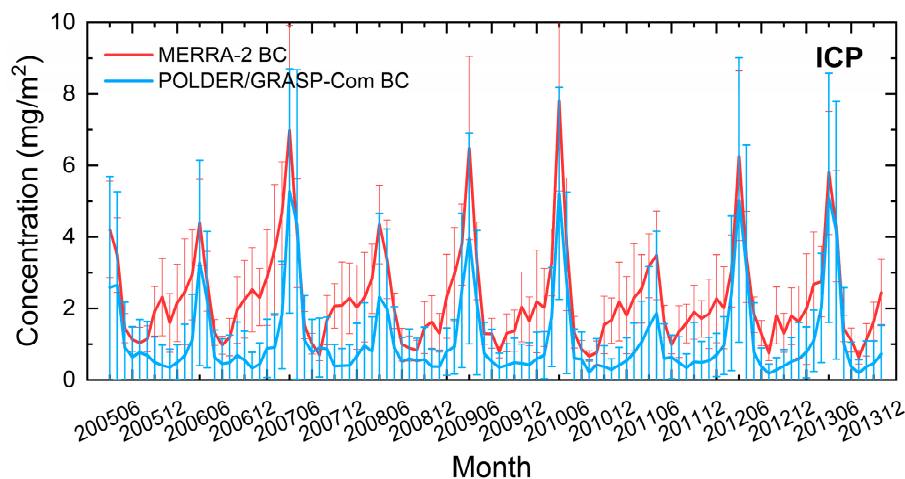


Figure 16. Same as Figure 13, but for Indo-China Peninsula (ICP) region.

3.2.5. North China Plain

Figure 17 presents the comparisons of BC column concentration between GRASP/Component BC retrieval and MERRA-2 BC product over the North China Plain (NCP) region. As shown in Figure 17, although both GRASP/Component BC retrieval and MERRA-2 BC product can describe the variation in monthly BC column concentration over the NCP region, large discrepancies are found for all months except in June. The correlation coefficient of $R = 0.46$ together with $RMSE = 3.88 \text{ mg/m}^2$ (in Table 4) is found between GRASP/Component BC retrieval and MERRA-2 BC product in the NCP region. The differences in regional means between these two products can be found in Table 5. We can see that over the NCP region, the BC column concentration of MERRA-2 is higher than those of GRASP/Component BC retrieval for all months. The absolute differences are larger than 3.5 mg/m^2 , and the relative difference is higher than 70%, except in June. It is noted that the absolute minimum difference and minimum relative difference (1.7 mg/m^2 and 31.3%, respectively) are recorded simultaneously in June when GRASP/Component retrieval presents well the strongest BC emission associated with the biomass burning of agricultural activities in the NCP region. The significant differences, to some extent, could be attributed to the emissions inventory assumption employed in models [30,31]. Specifically, anthropogenic BC emission in CEDS inventory does not describe the decreasing trend of BC in eastern China from 2006 to 2014 [30]. For instance, several anthropogenic aerosol emissions in the key regions of China have shown decreasing trends since 2006, such as anthropogenic black carbon (BC) emission has a statistically noteworthy trend of -1.4% per year in the Peking University (PKU) inventory. However, anthropogenic BC emission in Community Emissions Data System (CEDS) inventory shows an increasing trend of 2.7% over eastern China for the period 2006–2014, which is a complete reversal of the trend of PKU inventory. Therefore, the models that employ CEDS inventory cannot successfully capture the practical descending tendency [30]. Assimilated AOD observations in MERRA-2 cannot provide sufficient information and constraints on the fractions or content

of aerosol species. In addition, the satellite-derived GRASP/Component BC products in China had been validated by in situ measurements with a mean absolute difference of about $2.7 \mu\text{m}/\text{m}^3$, ranging from 0.09 to $7.8 \mu\text{m}/\text{m}^3$, and the relative difference of about 40%, ranging from 2.6% to 60%, respectively [41].

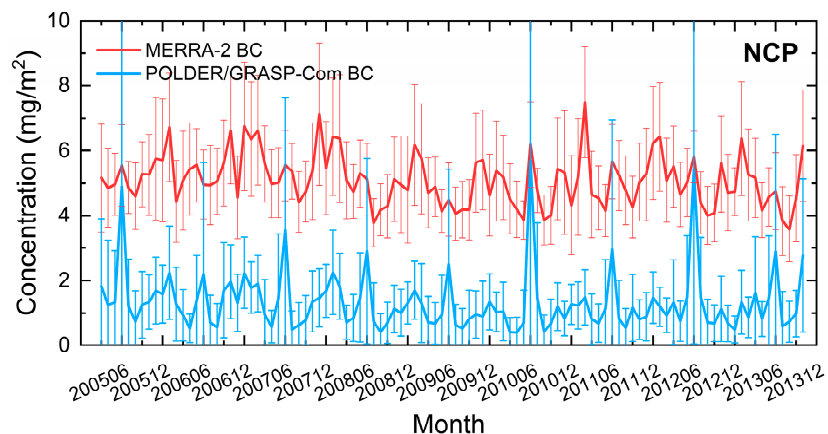


Figure 17. Same as Figure 13, but for North China Plain (NCP) region.

3.2.6. Northeast China and East Russia

Figure 18 presents the comparisons of BC column concentration over Northeast China and east of Russia (NCR) region between GRASP/Component BC retrieval and MERRA-2 BC product. It is worth mentioning that both GRASP/Component BC retrieval and MERRA-2 BC product can capture well the variation in monthly BC column concentration over the NCR region. Specifically, GRASP/Component BC retrieval and MERRA-2 BC product presents the highest BC column concentration in April and May, whereas low values in the other months. The correlation coefficient of $R = 0.68$ together with $\text{RMSE} = 0.75 \text{ mg}/\text{m}^2$ (in Table 4) are found between GRASP/Component BC retrieval and MERRA-2 BC product in the NCR region, which could be attributed to small variabilities throughout the year. The differences in regional means between these two products can be found in Table 5. We can see that over the NCR region, the BC column concentration of MERRA-2 is higher than those of GRASP/Component BC retrieval for all months except December. The maximum absolute difference and relative difference are obtained in July ($1.1 \text{ mg}/\text{m}^2$ and 67.4%, respectively), as well as the absolute minimum difference of $-0.2 \text{ mg}/\text{m}^2$ and minimum relative difference of -13.6% are also recorded simultaneously in December (negative values indicate MERRA-2 BC column concentration are lower than GRASP/Component BC column concentration).

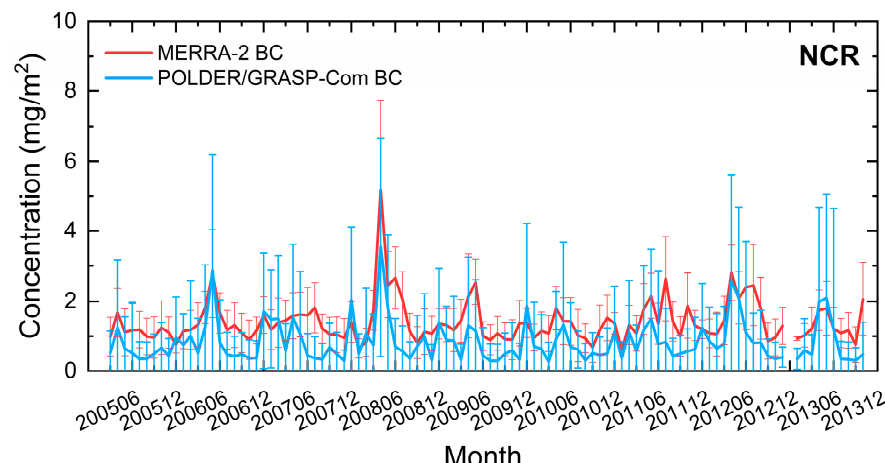


Figure 18. Same as Figure 13, but for Northeast China and east of Russia (NCR) region.

4. Conclusions

The aerosol assimilation system in MERRA-2 reanalysis data has been assessed and validated by many studies using the measurements of aerosol optical properties such as AOD over a regional or global scale. However, the evaluation of MERRA-2 aerosol component products is still not conducted globally due to the scarcity of aerosol component measurements on extensive temporal and spatial scales. This study presents a quantitative evaluation of the MERRA-2 reanalysis dust and BC column concentration using the independent satellite-measured aerosol component concentration retrievals, which are not assimilated by the MERRA-2 reanalysis system. Several dust emission resource regions and the critical downwind dust-dominated regions are selected for the comparisons of mineral dust column concentration globally, as well as the conducted BC comparisons in some key regions of interest for strong BC emission.

Generally, the performed analysis conducted in the key regions of interest globally highlights the agreement between MERRA-2 and GRASP/Component for the mineral dust and black carbon column concentration products, although some differences can be observed with reasonable explanations. It is critical to understand the behavior of MERRA-2 reanalysis component estimation and component retrievals derived from satellite observations.

The GRASP/Component and MERRA-2 reanalysis products show consistent temporal variation in dust column concentration over the dust emission resource regions, with the correlation coefficient varying from 0.91 to 0.80. MERRA-2 reanalysis dust products present higher column concentration than GRASP/Component dust retrievals with relative differences of about 40~70% over the African dust emission resource regions (SAH and BOD). However, over Asian dust emission resource regions (MIE, TAK, and GOB), the relative differences are mostly less than 40%, even for negative values in the TAK region.

Over the downwind dust-dominated regions, the similar temporal variations in dust column concentration are also reflected by both GRASP/Component dust retrievals and MERRA-2 reanalysis dust products, with the correlation coefficient varying from 0.98 to 0.84. MERRA-2 reanalysis dust products present higher column concentration than GRASP/Component dust retrievals with relative differences of about 20~50% over the downwind dust-dominated regions except for the BOB region. Most of the relative differences in the BOB region are negative and can even reach a value smaller than −150%.

Over the biomass burning and BC-affected areas in the globe, similar temporal variations in BC column concentration are represented by both GRASP/Component BC retrievals and MERRA-2 BC products with a correlation coefficient of about 0.70~0.90 except the NCP region. Higher column concentrations with relative differences of about 80% and lower column concentrations with relative differences of about −20% are presented by MERRA-2 reanalysis BC products compared to GRASP/Component BC retrievals.

We should point out that the statistics for the comparisons of monthly regional averaged concentration could indicate that both MERRA-2 products and GRASP/Component retrievals can capture well the temporal variations in dust and BC column concentration with a high correlation coefficient. Large differences and high correlation coefficients could be obtained when systematic biases exist. For instance, a high correlation coefficient and large RMSE are obtained for dust comparisons in SAH, BOD, and MIE. In this case, we should pay more caution with the regional applicability of MERRA-2 component products. Although the magnitudes of dust and BC column concentration described by GRASP/Component retrievals and MERRA-2 reanalysis dataset present non-negligible discrepancies in some key regions, the results are helpful for the understanding of MERRA-2 reanalysis component products in a new view and demonstrate a practical application of the satellite-based component retrievals. With the development of an inversion algorithm and independent measurement data, the reasons for these differences are expected to be addressed in the near future.

Author Contributions: Conceptualization, L.L. and H.C.; methodology, L.L.; Software, L.L. and X.S.; validation, L.L., H.C. and X.Z. (Xindan Zhang); formal analysis, K.G., Y.Z., H.Z. (Hujia Zhao) and H.Z. (Hengheng Zhao); investigation, Y.L. (Yuanxin Liang) and L.Z.; resources, Y.L. (Yadong Lei) and Z.W.; data curation, J.Z.; writing—original draft preparation, L.L.; writing—review and editing, H.C., K.G., Y.Z., Z.W. and X.Z. (Xiaoye Zhang); visualization, X.S.; supervision, H.C. All authors have read and agreed to the published version of the manuscript.

Funding: This research has been supported by the National Science Fund for Distinguished Young Scholars (41825011), the National Natural Science Foundation of China (41905117, 42105138, 42175153, 42030608, and 42275195), and the Foundation of the Chinese Academy of Meteorological Sciences (2021Y002). The component algorithm was developed as part of the Labex CaPPA project, which is funded by the Agence Nationale de la Recherche (grant no. ANR-LABX-0005-01).

Data Availability Statement: MERRA-2 dust and black carbon products are available at <http://disc.sci.gsfc.nasa.gov/mdi/> (accessed on 1 October 2022). GRASP/Component dust and black carbon retrievals are available at <https://www.grasp-open.com> and <https://doi.org/10.5281/zenodo.6395384> (accessed on 1 October 2022).

Acknowledgments: We would like to acknowledge the entire GRASP-OPEN team for the component retrievals. Special thanks to Oleg Dubovik and Yevegeny Derimian for the development of the component algorithm. The authors are also grateful to the MERRA-2 product team.

Conflicts of Interest: The authors declare no conflict of interest.

References

1. Zhang, J.; Reid, J.S. A decadal regional and global trend analysis of the aerosol optical depth using a data-assimilation grade over-water MODIS and Level 2 MISR aerosol products. *Atmos. Chem. Phys.* **2010**, *10*, 10949–10963. [[CrossRef](#)]
2. Yoon, J.; Burrows, J.P.; Vountas, M.; Von Hoyningen-Huene, W.; Chang, D.Y.; Richter, A.; Hilboll, A. Changes in atmospheric aerosol loading retrieved from space-based measurements during the past decade. *Atmos. Chem. Phys.* **2014**, *14*, 6881–6902. [[CrossRef](#)]
3. Alfaro-Contreras, R.; Zhang, J.; Reid, J.S.; Christopher, S. A study of 15-year aerosol optical thickness and direct shortwave aerosol radiative effect trends using MODIS, MISR, CALIOP and CERES. *Atmos. Chem. Phys.* **2017**, *17*, 13849–13868. [[CrossRef](#)]
4. Che, H.; Gui, K.; Xia, X.; Wang, Y.; Holben, B.N.; Goloub, P.; Cuevas-Agulló, E.; Wang, H.; Zheng, Y.; Zhao, H.; et al. Large contribution of meteorological factors to inter-decadal changes in regional aerosol optical depth. *Atmos. Chem. Phys.* **2019**, *19*, 10497–10523. [[CrossRef](#)]
5. Klingmüller, K.; Pozzer, A.; Metzger, S.; Stenchikov, G.L.; Lelieveld, J. Aerosol optical depth trend over the Middle East. *Atmos. Chem. Phys.* **2016**, *16*, 5063–5073. [[CrossRef](#)]
6. Floutsi, A.A.; Korras-Carraca, M.B.; Matsoukas, C.; Hatzianastassiou, N.; Biskos, G. Climatology and trends of aerosol optical depth over the Mediterranean basin during the last 12 years (2002–2014) based on Collection 006 MODIS-Aqua data. *Sci. Total Environ.* **2016**, *551–552*, 292–303. [[CrossRef](#)]
7. Remer, L.A.; Kleidman, R.G.; Levy, R.C.; Kaufman, Y.J.; Tanré, D.; Mattoo, S.; Martins, J.V.; Ichoku, C.; Koren, I.; Yu, H.; et al. Global aerosol climatology from the MODIS satellite sensors. *J. Geophys. Res. Atmos.* **2008**, *113*, D14S07. [[CrossRef](#)]
8. Prospero, J.M.; Ginoux, P.; Torres, O.; Nicholson, S.E.; Gill, T.E. Environmental characterization of global sources of atmospheric soil dust identified with the Nimbus 7 Total Ozone Mapping Spectrometer (TOMS) absorbing aerosol product. *Rev. Geophys.* **2002**, *40*, 1–31. [[CrossRef](#)]
9. Ginoux, P.; Prospero, J.M.; Gill, T.E.; Hsu, N.C.; Zhao, M. Global-scale attribution of anthropogenic and natural dust sources and their emission rates based on MODIS Deep Blue aerosol products. *Rev. Geophys.* **2012**, *50*, 1–36. [[CrossRef](#)]
10. Song, Q.; Zhang, Z.; Yu, H.; Ginoux, P.; Shen, J. Global dust optical depth climatology derived from CALIOP and MODIS aerosol retrievals on decadal timescales: Regional and interannual variability. *Atmos. Chem. Phys.* **2021**, *21*, 13369–13395. [[CrossRef](#)]
11. Xi, X.; Sokolik, I.N. Dust interannual variability and trend in Central Asia from 2000 to 2014 and their climatic linkages. *J. Geophys. Res. Atmos.* **2015**, *120*, 238. [[CrossRef](#)]
12. Notaro, M.; Yu, Y.; Kalashnikova, O.V. Regime shift in arabian dust activity, triggered by persistent fertile crescent drought. *J. Geophys. Res.* **2015**, *120*, 10229–10249. [[CrossRef](#)]
13. Lakshmi, N.B.; Babu, S.S.; Nair, V.S. Recent Regime Shifts in Mineral Dust Trends over South Asia from Long-Term CALIPSO Observations. *IEEE Trans. Geosci. Remote Sens.* **2019**, *57*, 4485–4489. [[CrossRef](#)]
14. Chen, D.; Liu, Z.; Schwartz, C.S.; Cetola, J.D.; Gu, Y.; Xue, L. The impact of aerosol optical depth assimilation on aerosol forecasts and radiative effects during a wild fire event over the United States. *Geosci. Model Dev.* **2014**, *7*, 2709–2715. [[CrossRef](#)]
15. Schwartz, C.S.; Liu, Z.; Lin, H.-C.; Cetola, J.D. Assimilating aerosol observations with a “hybrid” variational-ensemble data assimilation system. *J. Geophys. Res. Atmos.* **2014**, *119*, 4043–4069. [[CrossRef](#)]

16. McHenry, J.N.; Vukovich, J.M.; Hsu, N.C. Development and implementation of a remote-sensing and in situ data-assimilating version of CMAQ for operational PM2.5 forecasting. Part 1: MODIS aerosol optical depth (AOD) data-assimilation design and testing. *J. Air Waste Manag. Assoc.* **2015**, *65*, 1395–1412. [[CrossRef](#)]
17. Heidinger, A.K.; Foster, M.J.; Walther, A.; Zhao, X. The pathfinder atmospheres-extended avhrr climate dataset. *Bull. Am. Meteorol. Soc.* **2014**, *95*, 909–922. [[CrossRef](#)]
18. Kahn, R.A.; Gaitley, B.J.; Martonchik, J.V.; Diner, D.J.; Crean, K.A.; Holben, B. Multiangle Imaging Spectroradiometer (MISR) global aerosol optical depth validation based on 2 years of coincident Aerosol Robotic Network (AERONET) observations. *J. Geophys. Res. Atmos.* **2005**, *110*, D10S04. [[CrossRef](#)]
19. Holben, B.N.; Eck, T.F.; Slutsker, I.; Tanré, D.; Buis, J.P.; Setzer, A.; Vermote, E.; Reagan, J.A.; Kaufman, Y.J.; Nakajima, T.; et al. AERONET—A Federated Instrument Network and Data Archive for Aerosol Characterization. *Remote Sens. Environ.* **1998**, *66*, 1–16. [[CrossRef](#)]
20. Buchard, V.; Randles, C.A.; da Silva, A.M.; Darmenov, A.; Colarco, P.R.; Govindaraju, R.; Ferrare, R.; Hair, J.; Beyersdorf, A.J.; Ziembka, L.D.; et al. The MERRA-2 aerosol reanalysis, 1980 onward. Part II: Evaluation and case studies. *J. Clim.* **2017**, *30*, 6851–6872. [[CrossRef](#)]
21. Randles, C.A.; da Silva, A.M.; Buchard, V.; Colarco, P.R.; Darmenov, A.; Govindaraju, R.; Smirnov, A.; Holben, B.; Ferrare, R.; Hair, J.; et al. The MERRA-2 Aerosol Reanalysis, 1980 Onward. Part I: System Description and Data Assimilation Evaluation. *J. Clim.* **2017**, *30*, 6823–6850. [[CrossRef](#)] [[PubMed](#)]
22. Buchard, V.; da Silva, A.M.; Randles, C.A.; Colarco, P.; Ferrare, R.; Hair, J.; Hostetler, C.; Tackett, J.; Winker, D. Evaluation of the surface PM2.5 in Version 1 of the NASA MERRA Aerosol Reanalysis over the United States. *Atmos. Environ.* **2016**, *125*, 100–111. [[CrossRef](#)]
23. Buchard, V.; Da Silva, A.M.; Colarco, P.R.; Darmenov, A.; Randles, C.A.; Govindaraju, R.; Torres, O.; Campbell, J.; Spurr, R. Using the OMI aerosol index and absorption aerosol optical depth to evaluate the NASA MERRA Aerosol Reanalysis. *Atmos. Chem. Phys.* **2015**, *15*, 5743–5760. [[CrossRef](#)]
24. Giordano, L.; Brunner, D.; Flemming, J.; Hogrefe, C.; Im, U.; Bianconi, R.; Badia, A.; Balzarini, A.; Baró, R.; Chemel, C.; et al. Assessment of the MACC reanalysis and its influence as chemical boundary conditions for regional air quality modeling in AQMEII-2. *Atmos. Environ.* **2015**, *115*, 371–388. [[CrossRef](#)]
25. Bellouin, N.; Quaas, J.; Morcrette, J.J.; Boucher, O. Estimates of aerosol radiative forcing from the MACC re-analysis. *Atmos. Chem. Phys.* **2013**, *13*, 2045–2062. [[CrossRef](#)]
26. Reale, O.; Lau, K.M.; Da Silva, A.; Matsui, T. Impact of assimilated and interactive aerosol on tropical cyclogenesis. *Geophys. Res. Lett.* **2014**, *41*, 3282–3288. [[CrossRef](#)]
27. Inness, A.; Baier, F.; Benedetti, A.; Bouarar, I.; Chabriat, S.; Clark, H.; Clerbaux, C.; Coheur, P.; Engelen, R.J.; Errera, Q.; et al. The MACC reanalysis: An 8 yr data set of atmospheric composition. *Atmos. Chem. Phys.* **2013**, *13*, 4073–4109. [[CrossRef](#)]
28. Kinne, S.; Schulz, M.; Textor, C.; Guibert, S.; Balkanski, Y.; Bauer, S.E.; Berntsen, T.; Berglen, T.F.; Boucher, O.; Chin, M.; et al. An AeroCom initial assessment—Optical properties in aerosol component modules of global models. *Atmos. Chem. Phys.* **2006**, *6*, 1815–1834. [[CrossRef](#)]
29. Textor, C.; Schulz, M.; Guibert, S.; Kinne, S.; Balkanski, Y.; Bauer, S.; Berntsen, T.; Berglen, T.; Boucher, O.; Chin, M.; et al. Analysis and quantification of the diversities of aerosol life cycles within AeroCom. *Atmos. Chem. Phys.* **2006**, *6*, 1777–1813. [[CrossRef](#)]
30. Wang, Z.; Lin, L.; Xu, Y.; Che, H.; Zhang, X.; Zhang, H.; Dong, W.; Wang, C.; Gui, K.; Xie, B. Incorrect Asian aerosols affecting the attribution and projection of regional climate change in CMIP6 models. *NPJ Clim. Atmos. Sci.* **2021**, *4*, 1–8. [[CrossRef](#)]
31. Paulot, F.; Paynter, D.; Ginoux, P.; Naik, V.; Horowitz, L.W. Changes in the aerosol direct radiative forcing from 2001 to 2015: Observational constraints and regional mechanisms. *Atmos. Chem. Phys.* **2018**, *18*, 13265–13281. [[CrossRef](#)]
32. Riener, M.M.; Suarez, M.J.; Gelaro, R.; Todling, R.; Bacmeister, J.; Liu, E.; Bosilovich, M.G.; Schubert, S.D.; Takacs, L.; Kim, G.K.; et al. MERRA: NASA’s modern-era retrospective analysis for research and applications. *J. Clim.* **2011**, *24*, 3624–3648. [[CrossRef](#)]
33. Molod, A.; Takacs, L.; Suarez, M.; Bacmeister, J. Development of the GEOS-5 atmospheric general circulation model: Evolution from MERRA to MERRA2. *Geosci. Model Dev.* **2015**, *8*, 1339–1356. [[CrossRef](#)]
34. Wu, W.S.; Purser, R.J.; Parrish, D.F. Three-dimensional variational analysis with spatially inhomogeneous covariances. *Mon. Weather Rev.* **2002**, *130*, 2905–2916. [[CrossRef](#)]
35. Gelaro, R.; McCarty, W.; Suárez, M.J.; Todling, R.; Molod, A.; Takacs, L.; Randles, C.A.; Darmenov, A.; Bosilovich, M.G.; Reichle, R.; et al. The modern-era retrospective analysis for research and applications, version 2 (MERRA-2). *J. Clim.* **2017**, *30*, 5419–5454. [[CrossRef](#)]
36. Chin, M.; Ginoux, P.; Kinne, S.; Torres, O.; Holben, B.N.; Duncan, B.N.; Martin, R.V.; Logan, J.A.; Higurashi, A.; Nakajima, T. Tropospheric Aerosol Optical Thickness from the GOCART Model and Comparisons with Satellite and Sun Photometer Measurements. *J. Atmos. Sci.* **2002**, *59*, 461–483. [[CrossRef](#)]
37. Colarco, P.; Da Silva, A.; Chin, M.; Diehl, T. Online simulations of global aerosol distributions in the NASA GEOS-4 model and comparisons to satellite and ground-based aerosol optical depth. *J. Geophys. Res. Atmos.* **2010**, *115*, D14207. [[CrossRef](#)]
38. Tanré, D.; Bräon, F.M.; Deuzä, J.L.; Dubovik, O.; Ducos, F.; Franäois, P.; Goloub, P.; Herman, M.; Lifermann, A.; Waquet, F. Remote sensing of aerosols by using polarized, directional and spectral measurements within the A-Train: The PARASOL mission. *Atmos. Meas. Tech.* **2011**, *4*, 1383–1395. [[CrossRef](#)]

39. Li, L.; Derimian, Y.; Chen, C.; Zhang, X.; Che, H.; Schuster, G.L.; Fuertes, D.; Litvinov, P.; Lapyonok, T.; Lopatin, A.; et al. Climatology of aerosol component concentrations derived from multi-angular polarimetric POLDER-3 observations using GRASP algorithm. *Earth Syst. Sci. Data* **2022**, *14*, 3439–3469.
40. Li, L.; Dubovik, O.; Derimian, Y.; Schuster, G.L.; Lapyonok, T.; Litvinov, P.; Ducos, F.; Fuertes, D.; Chen, C.; Li, Z.; et al. Retrieval of aerosol components directly from satellite and ground-based measurements. *Atmos. Chem. Phys.* **2019**, *19*, 13409–13443. [[CrossRef](#)]
41. Duncan, B.N.; Martin, R.V.; Staudt, A.C.; Yevich, R.; Logan, J.A. Interannual and seasonal variability of biomass burning emissions constrained by satellite observations. *J. Geophys. Res.* **2003**, *D2*, 4100. [[CrossRef](#)]
42. Logothetis, S.-A.; Salamalikis, V.; Gkikas, A.; Kazadzis, S.; Amiridis, V.; Kazantzidis, A. 15-Year Variability of Desert Dust Optical Depth on Global and Regional Scales. *Atmos. Chem. Phys.* **2021**, *21*, 16499–16529. [[CrossRef](#)]
43. Li, L.; Che, H.; Derimian, Y.; Dubovik, O.; Schuster, G.L.; Chen, C.; Li, Q.; Wang, Y.; Guo, B.; Zhang, X. Retrievals of fine mode light-absorbing carbonaceous aerosols from POLDER/PARASOL observations over East and South Asia. *Remote Sens. Environ.* **2020**, *247*, 111913. [[CrossRef](#)]
44. Choobari, O.A.; Zawar-Reza, P.; Sturman, A. The global distribution of mineral dust and its impacts on the climate system: A review. *Atmos. Res.* **2014**, *138*, 152–165. [[CrossRef](#)]
45. Prospero, J.M.; Lamb, P.J. African Droughts and Dust Transport to the Caribbean: Climate Change Implications. *Science* **2003**, *302*, 1024–1027. [[CrossRef](#)]
46. Prospero, J.M.; Mayol-Bracero, O.L. Understanding the transport and impact of African dust on the Caribbean Basin. *Bull. Am. Meteorol. Soc.* **2013**, *94*, 1329–1337. [[CrossRef](#)]
47. Jingfeng, H.; Chidong, Z.; Prospero, J.M. African dust outbreaks: A satellite perspective of temporal and spatial variability over the tropical Atlantic Ocean. *J. Geophys. Res. Atmos.* **2010**, *115*, D05202.
48. Mona, L.; Amodeo, A.; Pandolfi, M.; Pappalardo, G. Saharan dust intrusions in the Mediterranean area: Three years of Raman lidar measurements. *J. Geophys. Res. Atmos.* **2006**, *111*, D16203. [[CrossRef](#)]
49. Gkikas, A.; Basart, S.; Hatzianastassiou, N.; Marinou, E.; Amiridis, V.; Kazadzis, S.; Pey, J.; Querol, X.; Jorba, O.; Gasso, S.; et al. Mediterranean intense desert dust outbreaks and their vertical structure based on remote sensing data. *Atmos. Chem. Phys.* **2016**, *16*, 8609–8642. [[CrossRef](#)]
50. Pozzer, A.; De Meij, A.; Yoon, J.; Tost, H.; Georgoulias, A.K.; Astitha, M. AOD trends during 2001–2010 from observations and model simulations. *Atmos. Chem. Phys.* **2015**, *15*, 5521–5535. [[CrossRef](#)]
51. Yu, Y.; Notaro, M.; Liu, Z.; Wang, F.; Alkolibi, F.; Fadda, E.; Bakhrjy, F. Climatic controls on the interannual to decadal variability in Saudi Arabian dust activity: Toward the development of a seasonal dust prediction model. *J. Geophys. Res.* **2015**, *120*, 1739–1758. [[CrossRef](#)]
52. Gkikas, A.; Proestakis, E.; Amiridis, V.; Kazadzis, S.; Di Tomaso, E.; Marinou, E.; Hatzianastassiou, N.; Kok, J.F.; García-Pando, C.P. Quantification of the dust optical depth across spatiotemporal scales with the MIDAS global dataset (2003–2017). *Atmos. Chem. Phys.* **2022**, *22*, 3553–3578. [[CrossRef](#)]
53. Evan, A.T.; Flamant, C.; Gaetani, M.; Guichard, F. The past, present and future of African dust. *Nature* **2016**, *531*, 493–495. [[CrossRef](#)] [[PubMed](#)]
54. Pan, B.; Wang, Y.; Hu, J.; Lin, Y.; Hsieh, J.S.; Logan, T.; Feng, X.; Jiang, J.H.; Yung, Y.L.; Zhang, R. Impacts of Saharan dust on Atlantic regional climate and implications for tropical cyclones. *J. Clim.* **2018**, *31*, 7621–7644. [[CrossRef](#)]
55. Xian, P.; Klotzbach, P.J.; Dunion, J.P.; Janiga, M.A.; Reid, J.S.; Colarco, P.R.; Kipling, Z. Revisiting the relationship between Atlantic dust and tropical cyclone activity using aerosol optical depth reanalyses: 2003–2018. *Atmos. Chem. Phys.* **2020**, *20*, 15357–15378. [[CrossRef](#)]
56. Gläser, G.; Wernli, H.; Kerkweg, A.; Teubler, F. The transatlantic dust transport from North Africa to the Americas—Its characteristics and source regions. *J. Geophys. Res.* **2015**, *120*, 11231–11235. [[CrossRef](#)]
57. Prospero, J.M.; Collard, F.-X.; Molinié, J.; Jeannot, A. Characterizing the annual cycle of African dust transport to the Caribbean Basin and South America and its impact on the environment and air quality. *Global Biogeochem. Cycles* **2014**, *28*, 757–773. [[CrossRef](#)]
58. Washington, R.; Todd, M.C.; Engelstaedter, S.; Mbainayel, S.; Mitchell, F. Dust and the low-level circulation over the Bodélé Depression, Chad: Observations from BoDEx 2005. *J. Geophys. Res. Atmos.* **2006**, *111*, D03201. [[CrossRef](#)]
59. Gkikas, A.; Hatzianastassiou, N.; Mihalopoulos, N.; Katsoulis, V.; Kazadzis, S.; Pey, J.; Querol, X.; Torres, O. The regime of intense desert dust episodes in the Mediterranean based on contemporary satellite observations and ground measurements. *Atmos. Chem. Phys.* **2013**, *13*, 12135–12154. [[CrossRef](#)]
60. Gkikas, A.; Houssos, E.E.; Lolis, C.J.; Bartzokas, A.; Mihalopoulos, N.; Hatzianastassiou, N. Atmospheric circulation evolution related to desert-dust episodes over the Mediterranean. *Q. J. R. Meteorol. Soc.* **2015**, *141*, 1634–1645. [[CrossRef](#)]
61. Shi, L.; Zhang, J.; Yao, F.; Zhang, D.; Guo, H. Drivers to dust emissions over dust belt from 1980 to 2018 and their variation in two global warming phases. *Sci. Total Environ.* **2021**, *767*, 144860. [[CrossRef](#)] [[PubMed](#)]

Disclaimer/Publisher’s Note: The statements, opinions and data contained in all publications are solely those of the individual author(s) and contributor(s) and not of MDPI and/or the editor(s). MDPI and/or the editor(s) disclaim responsibility for any injury to people or property resulting from any ideas, methods, instructions or products referred to in the content.